Downlink Channel Covariance Matrix Estimation in FDD Systems

Salime Bameri, Khalid Almahrog, Ramy H. Gohary, Amr El-Keyi, and Yahia Ahmed
{salimebameri, khalidalmahrog, gohary}@sce.carleton.ca
{amr.el-keyi, yahia.ahmed}@ericsson.com

***Abstract*—This paper considers frequency division duplexing massive multiple-input multiple-output systems in which the base station (BS) is equipped with either a uniform linear antenna array (ULA) or a uniform rectangular antenna array (URA). For these systems, we develop novel uplink-to-downlink channel covariance estimation schemes. These schemes can be expressed in the form of easy-to-implement affine transformations which depend only on the uplink and downlink carrier frequencies, and the BS array configurations. We derive upper bounds on the estimation errors, and we use these bounds to show that the accuracy of the proposed schemes increases with the number ULA/URA antennas, the compactness and differentiability class of the periodic extension of a non-linearly transformed version of the angular power spread. Performance superiority of the proposed schemes over their existing counterparts is confirmed through numerical simulations.**

I. Introduction

The massive multiple-input multiple-output (mMIMO) technology is one of the key enablers for 5G and beyond networks [1]. In this technology, users equipped with a small number, e.g., one or two, antennas communicate with a base station (BS) equipped with potentially hundreds of antennas. Such a large number of antennas enables the BS to communicate reliably within a given bandwidth at aggregate rates of hundreds of bits per channel use (bpcu) [2], [3], [4].

Emerging cellular systems are expected to operate either in the time division duplexing (TDD) or in the frequency division duplexing (FDD) mode. In TDD, the uplink (UL) and downlink (DL) transmissions occur within the same frequency band, but during different time intervals. If these intervals lie within the same coherence time of the channel, the UL channel state information (CSI) and its DL counterpart are approximately equal, giving rise to the so-called channel reciprocity [5]. In contrast with TDD, in the FDD mode, the UL and DL transmissions occur simultaneously in different frequency bands [6] that are potentially separated by a large spectral gap. This gap results in significant discrepancies between the UL and DL CSIs, thereby invalidating the channel reciprocity assumption.

Acquiring DL CSI in FDD mMIMO systems must overcome two challenges. The first challenge arises due to the large number of antennas at the BS and is common between TDD and FDD mMIMO systems. To see this, we note that the time required for transmitting the pilot symbols required to assist the receiver in estimating the CSI is proportional to the number of transmit antennas [7], [8]. Hence, while it is easy for the BS to acquire the UL CSI, acquiring the DL CSI is significantly more challenging. In particular, the significant overhead required to estimate the DL CSI may infringe on the resources available for actual communication, reducing the system spectral efficiency, and potentially causing the pilot transmission time to exceed the channel coherence time [9], [10]. The second challenge encountered in acquiring the DL CSI of FDD mMIMO systems is specific to these systems and arises from the fact that channel reciprocity characteristic of TDD systems [5] is not present in FDD ones. This difficulty is more pronounced when the spectral gap between the UL and DL channels is large. One approach to achieve effective communication despite the lack of DL CSI is to replace this CSI with its second order statistics, i.e., the spatial DL channel covariance matrix (DCCM) [11], [12].

Estimating the DCCM in FDD mMIMO systems without using DL pilots has been considered in e.g., [13]–[20]. Therein, the DCCMs are inferred from the corresponding uplink channel covariance matrices (UCCMs). For example, the scheme proposed in [19] uses a dictionary of known UCCM-DCCM pairs to estimate a DCCM whenever a new UCCM estimate becomes available. The DCCM estimates are refined by interpolating between the entries of the dictionary. Another class of techniques for estimating DCCMs without DL pilots relies on the fact that both FDD and TDD systems feature a form of reciprocity in the angular domain. In particular, signal propagation analysis and practical measurements suggest that the angular distribution of power observed by the antenna array at the receiver, which is known as the angular power spectrum (APS), is much less sensitive to variations in frequency than the actual CSI [21]. This partial insensitivity plays a key role in facilitating the estimation of the DCCM from the UCCM.

In contrast with the technique in [19], APS reciprocity has been exploited by several schemes for estimating DCCMs from their UCCM counterparts in FDD mMIMO systems with uniform linear arrays (ULAs) [13]–[19] and with uniform rectangular arrays (URAs) [20]. These schemes can be classified into two classes viz., APS-Explicit and APS-Implicit schemes.

APS-Explicit schemes use the UCCM to estimate the APS and subsequently use this APS to estimate the DCCM [13], [14]. The explicit estimation of the APS results in high computational complexity especially for a large number of array antennas. Therefore, scalability is the main challenge for these schemes. For instance, in [13], [14], the UCCM is used in optimization framework to obtain estimates of the APS at a large number of angles that are uniformly distributed on the

angular span of the antenna array. The APS is reconstructed from the estimates provided by the optimization framework and is subsequently used to obtain the DCCM. The performance of this scheme depends heavily on the choice of the number of angles at which the APS is estimated; the larger this number the more accurate the estimate of the DCCM. Unfortunately, choosing a large number for the angles at which the APS is estimated results in an impractical computation complexity. Another limitation of this scheme is that it cannot be used when the enter-antenna spacing is larger than half the DL carrier wavelength.

Unlike their APS-Explicit counterparts, APS-Implicit schemes directly transform the UCCM to a DCCM estimate without estimating the APS explicitly. For instance, the scheme proposed in [18] uses APS reciprocity to estimate the DCCM by a linear frequency calibration transformation of the UCCM samples. Another technique that uses a similar philosophy is the one proposed in [16]. In that scheme, the APS is represented as a linear transformation of the UCCM samples. Using another linear map, the APS is transformed to obtain an estimate of the DCCM. The composition of the two linear transformations is equivalent to one linear transformation that maps the UCCM to the DCCM without explicitly estimating the APS. The transformation matrices of the schemes in [18] and [16] are completely determined by the array geometry and the carrier frequencies, i.e., they can be computed offline and stored for future use; however, obtaining these matrices involves the evaluation of a numerical integration for each element of those matrices, which is computationally demanding. In [17], APS reciprocity is used to show that DCCM samples can be obtained by sampling the UCCM at a factor determined by the ratio of DL-to-UL carrier frequencies. The DCCM is reconstructed by interpolating these samples using cubic splines. One of drawbacks of this scheme is that it requires the interpolation operations to be repeated every time the APS of the channel changes. In other words, no closed-form transformation that can be computed offline independently of the channel and can be used repeatedly is available. Furthermore, this scheme uses separate interpolation operations for the amplitudes and the phases of the UCCM samples which adds to its complexity.

In this paper, we propose novel UCCM-to-DCCM transformation schemes for FDD mMIMO systems equipped with ULAs and URAs. These schemes exploit the properties of the respective channel covariance matrices to improve estimation accuracy and reduce computational complexity. In particular, following the standard approach, the UCCM corresponding to ULAs and URAs are estimated using UL pilots [13], [16], [18]. Based on the periodicity of the APS, we show that particular elements of the UCCM can be regarded as the coefficients of a truncated Fourier series of a periodic extension of a nonlinearly transformed version of the APS. Such a transformation is in contrast with the linear transformations proposed in [18] and [16]. The truncated Fourier series representation enables us to obtain a continuous approximation of the transformed APS. Invoking reciprocity, the continuous approximation is used to obtain closed-form estimates of the entries of the DCCM. These estimates can be regarded as samples of the Whittaker–Shannon (sinc) interpolated UCCM [22]. Curiously, this interpolating-sampling process can be represented as a linear transformation that maps the estimates of UCCM elements to estimates of the DCCM. Analytical upper bounds on the estimation errors of the proposed schemes are derived to expose their dependence on the number of antennas, antenna spacing, and APS support and differentiability.

The proposed schemes feature the following advantages. First, in contrast with the scheme in [13], the accuracy of the proposed schemes improves with the increase in the number of ULA/URA antennas for any spacing between the antenna elements. This feature is observed in [16] only when the spacing between the array elements is equal to half the UL wavelength. In particular, under certain conditions, the DCCMs estimated via the proposed schemes approach the true DCCMs as the number of antennas goes to infinity. In addition to this advantage, our analysis shows that the accuracy of the proposed schemes not only depends on the number of antennas, but also on the compactness and differentiability class to which the APS belongs. In particular, highly differential APSs with narrow support will result in more accurate DCCM estimation than less differentiable APSs with wider support. This is because the accuracy of the Whittaker–Shannon interpolation used to implicitly reconstruct the APS improves with the number of array antennas. Moreover, for an infinite number of antennas, the Whittaker–Shannon interpolation uniquely and completely determines the DCCM. The second advantage of the proposed schemes is that they exhibit a lower computational complexity than their existing counterparts. This computational advantage stems from the fact that these schemes make use of the Toeplitz and block Toeplitz structures of the ULA and URA channel covariance matrices to pick specific elements of the UCCM and to use these elements to obtain the DCCM. This is in sharp contrast to other schemes that use all UCCM elements to obtain the DCCM [16], [18], [19]. In particular, whereas the number of UCCM elements needed for the scheme in [16] grows quadratically with the number of antennas, this number grows only linearly in the proposed schemes. The third advantage of the proposed schemes is that their implementation can be cast in the form of linear transformations that depend solely on the ratio between the UL and DL carrier frequencies and the geometry of the antenna array, but not on the explicit APS. This is in contrast with the scheme in [13], [23], which requires solving an optimization problem that depends not only on these parameters, but also on the APS and UCCM estimates. Hence, unlike the method in [13], [23], the transformations underlying the proposed schemes can be computed offline and stored for future use, irrespective of the APS of the channel. In addition, the elements of the transformation matrix of our schemes are samples of the closed-form sinc functions for both ULA and URA. This is in contrast with the scheme proposed in [18] and [16] wherein the computation of transformation matrix elements involves evaluating numerical integration. An exception to this observation is the scheme proposed in [16] for ULAs. Finally, as demonstrated by numerical simulations, the proposed schemes exhibit superior performance over existing ones when the number of antennas is large.

The paper is organized as follows. The system model for ULA and URA is presented in Section II. Section III gives the details of the proposed schemes. Simulation results are provided in Section IV, and Section V concludes the paper.

Notations: Bold upper and lower case letters will be used to denote matrices and column vectors, respectively. The transpose, complex conjugate and Hermitian of a matrix $\boldsymbol{A}$ will be denoted by, $\boldsymbol{A}^T$, $\boldsymbol{A}^*$ and $\boldsymbol{A}^\dagger$, respectively. The all one column vector of dimension N will be denoted by $\mathbf{1}_N$. The p,q-th entry of $\boldsymbol{A}$ will be denoted by $[\boldsymbol{A}]_{p,q}$, whereas the j,k-th entry of the p,q-th block of a block matrix $\boldsymbol{Q}$ will be denoted by $[\boldsymbol{Q}]_{(p,q),(j,k)}$. Finally, we will use $f(x) = o\big(g(x)\big)$ to imply that $\lim_{x\to\infty} \frac{f(x)}{g(x)} = 0$.

II. System Model

In this paper, we consider an mMIMO FDD system composed of single antenna users communicating with a BS equipped with multiple antennas arranged in either a ULA or a URA configuration over narrowband channels, that is, the UL and DL transmission bandwidths are much less that their respective carrier frequencies. The UL and DL carrier frequencies are denoted by $f^{(ul)}$ and $f^{(dl)}$, respectively, and the ratio of these frequencies is denoted by $\alpha = \frac{f^{(dl)}}{f^{(ul)}}$.

We assume that both the UL and DL channels are multipath frequency-flat following the wide sense stationary uncorrelated scattering (WSSUS) model. In this model, the channel correlation function is time-invariant and the scatterers with different angles of arrival (AoAs) are uncorrelated [24], [25]. Using this model, the UL and DL channel vectors and covariance matrices for the ULA and URA cases are described in the following subsections.

A. ULA System Model

In this subsection, we assume that the BS is equipped with an M-antenna ULA, $M \gg 1$, with uniform antenna spacing denoted by L, cf. Figure 1a. We denote the complex channel gain by $\zeta(t,\theta)$, where θ is the AoA of the radio-frequency wave incident on the ULA. Following the WSSUS model, the channel gain autocorrelation function is given by [23], [26]:

$$E\left\{\zeta(t,\theta)\zeta^*(t',\theta')\right\} = \eta(t-t')\rho(\theta-\theta')\delta(\theta-\theta'), \qquad (1)$$

where the temporal correlation function, $\eta(\cdot)$, satisfies $\eta(0) = 1$ and $\eta(\tau) \approx 0$ for τ greater than the coherence time of the channel, and the APS, $\rho(\theta) \in \mathbb{R}_+$, describing the channel power distribution in the angular domain satisfies $\int_{-\pi}^{\pi} \rho(\theta)\, d\theta = 1$. To obtain expressions for the UCCM and DCCM in this case, we recall that the UL/DL channel vector $\boldsymbol{h}^{(i)}(t) \in \mathbb{C}^M$, $i \in \{ul, dl\}$, between each user and the M-antenna BS can be modeled as [26], [27]

$$\boldsymbol{h}^{(i)}(t) = \int_{-\pi}^{\pi} \zeta(t,\theta)\boldsymbol{a}^{(i)}(\theta)d\theta, \qquad i \in \{ul, dl\}, \qquad (2)$$

where $\boldsymbol{a}^{(i)}(\theta) \in \mathbb{C}^M$ is the ULA UL/DL steering vector, which is given by, $i \in \{ul, dl\}$:

$$\boldsymbol{a}^{(i)}(\theta) = \begin{bmatrix} 1 & e^{\jmath 2\pi \frac{L}{\lambda^{(i)}} \sin(\theta)} & \dots & e^{\jmath 2\pi \frac{L}{\lambda^{(i)}} (M-1)\sin(\theta)} \end{bmatrix}^T, \qquad (3)$$

where $\lambda^{(i)} = \frac{f^{(i)}}{c_0}$ is the UL/DL wavelength; c_0 is the speed of light.

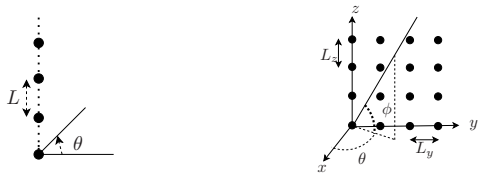

(a) ULA (b) URA

Fig. 1: ULA and URA configurations.

Using the channel vector given in (2) along with (1), the spatial UCCM/DCCM $\boldsymbol{R}^{(i)} \in \mathbb{C}^{M\times M}$ can be expressed as [13], [16], [18]:

$$\begin{aligned}\boldsymbol{R}^{(i)} &= E\left\{\boldsymbol{h}^{(i)}(t)\boldsymbol{h}^{(i)^\dagger}(t)\right\}, \\ &= \int_{-\pi}^{\pi} \rho(\theta)\boldsymbol{a}^{(i)}(\theta)\boldsymbol{a}^{(i)^\dagger}(\theta)\, d\theta, \quad i \in \{ul, dl\}. \end{aligned} \qquad (4)$$

Using (3) and (4), the p,q-th element of the ULA UCCM/DCCM can be expressed as:

$$\begin{aligned}[\boldsymbol{R}^{(i)}]_{p,q} &= \int_{-\pi}^{\pi} \rho(\theta) e^{\jmath \frac{2\pi}{\lambda^{(i)}} L(p-q)\sin(\theta)}\, d\theta, \\ & p,q = 1,\dots,M,\ i \in \{ul, dl\}. \end{aligned} \qquad (5)$$

We make the standard assumption that the APS, $\rho(\theta)$, is frequency-independent and unknown at both the user and the BS. In contrast, the steering vector, $\boldsymbol{a}^{(i)}(\theta)$ in (3) is frequency-dependent and known at both the user and the BS [13], [18]. (For notational convenience, the dependence of $\boldsymbol{a}^{(i)}(\theta)$ on $f^{(i)}$ has been suppressed throughout.) This assumption along with (4) show that, in FDD systems, $\boldsymbol{R}^{(ul)}$ and $\boldsymbol{R}^{(dl)}$ are inherently related. This is the key property which will enable us to estimate the DCCM using the observed UCCM.

Using the channel covariance matrices in (4) and the steering vectors in (3), it can be readily shown that, for a ULA system, channel covariance matrices are Hermitian, i.e. $\boldsymbol{R}^{(i)^\dagger} = \boldsymbol{R}^{(i)}$, positive semi-definite, i.e., $\boldsymbol{x}^\dagger \boldsymbol{R}^{(i)} \boldsymbol{x} \geq 0$ for any $\boldsymbol{x} \in \mathbb{C}^M$, and Toeplitz, i.e., $[\boldsymbol{R}^{(i)}]_{p,q} = [\boldsymbol{R}^{(i)}]_{p+1,q+1}$, $p,q \in \{1,\dots,M-1\}$. These properties will enable us to construct the entire covariance matrix using only the elements of the first column, thereby yielding valuable reduction in the computational complexity, specially when M is large.

B. URA System Model

In this subsection, we assume that the BS is equipped with an $M \times N$-antenna URA located in the yz plane. In particular, the URA consists of N L_y-uniformly-spaced antennas in each row and M L_z-uniformly-spaced antennas in each column, cf. Figure 1b.

Using a procedure similar to that used in Section II-A, an expression analogous to (4) can be obtained for the URA UCCM/DCCM, $\boldsymbol{R}^{(i)} \in \mathbb{C}^{MN\times MN}$, $i \in \{ul, dl\}$. In particular, we have, $i \in \{ul, dl\}$, [28]

$$\boldsymbol{R}^{(i)} = \int_{-\frac{\pi}{2}}^{\frac{\pi}{2}} \int_{-\pi}^{\pi} \rho(\theta,\phi)\boldsymbol{a}^{(i)}(\theta,\phi)\boldsymbol{a}^{(i)^\dagger}(\theta,\phi)\, d\theta\, d\phi, \qquad (6)$$

where θ and ϕ are the azimuth and elevation AoAs, respectively, and $\rho(\theta,\phi) \in \mathbb{R}_+$ is the URA APS which satisfies $\int_{-\frac{\pi}{2}}^{\frac{\pi}{2}}\int_{-\pi}^{\pi}\rho(\theta,\phi)d\theta d\phi = 1$. In this expression, $\boldsymbol{a}^{(i)}(\theta,\phi) \in \mathbb{C}^{MN}$ is the UL/DL URA steering vector which is given by:

$$\boldsymbol{a}^{(i)}(\theta,\phi) = \left[\boldsymbol{a}_1^{(i)^T}(\theta,\phi) \quad \dots \quad \boldsymbol{a}_N^{(i)^T}(\theta,\phi)\right]^T,\ i \in \{ul,dl\}, \tag{7}$$

where $\boldsymbol{a}_n^{(i)}(\theta,\phi) \in \mathbb{C}^M$, $n = 1\dots,N$, is the steering vector corresponding to the n-th column of the URA and is given by

$$\boldsymbol{a}_n^{(i)}(\theta,\phi) = \left[a_{n,1}^{(i)} \quad \dots \quad a_{n,M}^{(i)}\right]^T,\ i\in \{ul,dl\}. \tag{8}$$

The m-th entry of the n-th steering vector, $a_{m,n}^{(i)}$, corresponding to the n,m element of the URA antenna grid, $n \in \{1,\dots,N\}$, $m \in \{1,\dots,M\}$, is given by, $i \in \{ul,dl\}$:

$$a_{n,m}^{(i)} = e^{\jmath\frac{2\pi}{\lambda^{(i)}}\left((n-1)L_y\sin(\theta)\cos(\phi)+(m-1)L_z\sin(\phi)\right)}, \tag{9}$$

Using (6), (7) and (8) and letting $p = (n_1-1)M+m_1$ and $q = (n_2-1)M+m_2$, $n_1,n_2 = 1,\dots,N$, $m_1,m_2 = 1,\dots,M$, the p,q-th entry of the URA UCCM/DCCM can be expressed as, $i \in \{ul,dl\}$:

$$\begin{aligned}[\boldsymbol{R}^{(i)}]_{p,q} &= \int_{-\frac{\pi}{2}}^{\frac{\pi}{2}}\int_{-\pi}^{\pi}\rho(\theta,\phi)e^{\jmath\frac{2\pi}{\lambda^{(i)}}D(\theta,\phi)}\,d\theta\,d\phi,\\ D_{n_1n_2m_1m_2}(\theta,\phi) &= (n_1-n_2)L_y\sin(\theta)\cos(\phi)\\ &\quad + (m_1-m_2)L_z\sin(\phi),\end{aligned} \tag{10}$$

Analogous to the ULA case, we assume that the APS, $\rho(\theta,\phi)$, is frequency-independent and unknown, whereas the steering vectors $\boldsymbol{a}^{(i)}(\theta,\phi)$, $i \in \{ul,dl\}$ in (7) are frequency-dependent and known. Analogous to the ULA case, it can be seen from (6) that $\boldsymbol{R}^{(ul)}$ and $\boldsymbol{R}^{(dl)}$ are inherently related, which will enable us to estimate the DCCM using the observed UCCM.

III. Proposed DCCM Estimation Schemes For ULA and URA Systems

We propose novel DCCM estimation schemes for ULA and URA systems. The main philosophy of these schemes is to express particular elements of the UCCM as the coefficients of a truncated Fourier series of a periodic extension of a non-linearly transformed version of the APS. These truncated Fourier series coefficients allow us to obtain a continuous approximation of the transformed APS, which is subsequently used to obtain closed-form estimates of the DCCM entries.

Analytical upper bounds on the estimation errors of the proposed schemes are derived to expose their dependence on the number of antennas, antenna spacing, and APS support and differentiability. In particular, we show that the accuracy of these schemes increases when the number of ULA/URA antennas is large and the transformed APS is highly differentiable with support span less than 2π. Under these conditions, the proposed schemes exhibit superior performance at a significantly less computational cost than their existing counterparts.

A. Proposed Scheme for ULA

Towards developing the proposed scheme, we use (4) to provide new characterizations of the UCCM and DCCM, which are provided in the following lemma.

Lemma 1: Let $\lambda^{(ul)}$ be the wavelength of the UL transmission from a single-antenna user to a BS equipped with a ULA composed of M L-uniformly-spaced antennas. Let $\rho(\theta)$ be the APS, $\gamma = \frac{L}{\lambda^{(ul)}}$, and let $\alpha = \frac{f^{(dl)}}{f^{(ul)}}$. Furthermore, let

$$\rho'(u) = \frac{\rho(\arcsin\frac{u}{2\pi\gamma}) + \rho(\pi-\arcsin\frac{u}{2\pi\gamma})}{\sqrt{\gamma^2-(\frac{u}{2\pi})^2}}, \tag{11}$$

and let $\mu_m^{(ul)}(u) = mu$ and $\mu_m^{(dl)}(u) = \alpha\mu_m^{(ul)}(u)$. Using this notation, the p,q-th entry of the UCCM/DCCM, $[\boldsymbol{R}^{(i)}]_{p,q}$, $i \in \{ul,dl\}$, can be expressed as, $p,q = 1,\dots,M$:

$$[\boldsymbol{R}^{(i)}]_{p,q} = \frac{1}{2\pi}\int_{-\pi}^{\pi}\vartheta(u)e^{\jmath\mu_{p-q}^{(i)}(u)}\,du + \delta_{p-q}^{(i)}, \tag{12}$$

where

$$\vartheta(u) = \begin{cases}\rho'(u) & |u| \le \min(\pi,2\pi\gamma),\\ 0 & \text{otherwise},\end{cases} \tag{13}$$

and

$$\delta_m^{(i)} = \frac{1}{2\pi}\int_{-2\pi\gamma}^{2\pi\gamma}\rho'(u)e^{\jmath\mu_m^{(i)}(u)}\,du - \frac{1}{2\pi}\int_{-\pi}^{\pi}\vartheta(u)e^{\jmath\mu_m^{(i)}(u)}\,du. \tag{14}$$

Proof: See Appendix A. ∎

We note that $\rho'(\cdot)$ in (11) constitutes a non-linear transformation of the APS, $\rho(\cdot)$. Furthermore, whereas $\rho(\cdot)$ is periodic with period 2π, $\rho'(\cdot)$ is aperiodic. However, from Appendix A, it can be seen that the variable u in (11) is given by $u = 2\pi\gamma\sin(\theta)$. Hence, every period of $\rho(\theta)$ maps to the aperiodic function $\rho'(u)$ with $u \in [-2\pi\gamma, 2\pi\gamma]$ in (11). When $\gamma \le \frac{1}{2}$, the support of $\rho'(u)$ is within the interval $[-\pi,\pi)$, but when $\gamma > \frac{1}{2}$, the support extends beyond this interval. The first term on the right hand side (RHS) of (12) accounts for $\rho'(u)$ in the interval $(-\pi,\pi)$ whereas the second term, i.e., $\delta_{p-q}^{(i)}$ which is defined in (14), accounts for $\rho'(u)$ beyond $(-\pi,\pi)$. From (14), it can be readily seen that, when $\gamma \le \frac{1}{2}$, $\delta_{p-q}^{(i)} = 0$, and when $\gamma > \frac{1}{2}$, $\delta_{p-q}^{(i)} \neq 0$, unless $\rho'(\cdot) = 0$ outside the interval $(-\pi,\pi)$. An illustration of the functions $\rho'(u)$ and $\vartheta(u)$ for $\gamma > \frac{1}{2}$ is given in Figure 2.

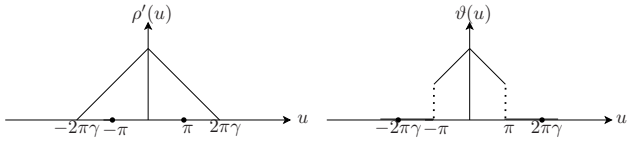

Fig. 2: $\rho'(u)$ and $\vartheta(u)$ for $\gamma > \frac{1}{2}$

The characterization of $\boldsymbol{R}^{(i)}$ in Lemma 1 enables us to use the entries of the UCCM to obtain a continuous approximation of a periodic extension of $\vartheta(u)$. This approximation will be used to provide closed form estimates of the DCCM elements. Since the DCCM is Toeplitz and Hermitian (cf. Section II-A), it can be uniquely reconstructed from its first

column. Considering (12), the first column elements of the UCCM and the DCCM can be described by

$$r_m^{(i)} = [\boldsymbol{R}^{(i)}]_{p,q}\Big|_{m=p-q}, \quad m = 0, \ldots, (M-1), \qquad i \in \{ul, dl\}, \tag{15}$$

that is, $\{r_m^{(i)}\}$ are obtained from (12) by substituting m for $p-q$. Using this notation, the elements of the first row of the UCCM and the DCCM are given by $r_m^{(i)}$, $m = -(M-1), \ldots, 0$, and $i \in \{ul, dl\}$. In the following theorem, we will use this notation to obtain $\{r_m^{(dl)}\}$ from $\{r_m^{(ul)}\}$.

Theorem 1: For an M-antenna ULA, let $\hat{\boldsymbol{r}}^{(ul)}$ contain the first row and the first column of the UCCM, i.e., $\hat{\boldsymbol{r}}^{(ul)} = \begin{bmatrix} r_{-(M-1)}^{(ul)} \cdots r_0^{(ul)} \cdots r_{(M-1)}^{(ul)} \end{bmatrix}^T$, and let $\boldsymbol{r}^{(dl)}$ contain the first column of the DCCM, i.e., $\boldsymbol{r}^{(dl)} = \begin{bmatrix} r_0^{(dl)} \cdots r_{(M-1)}^{(dl)} \end{bmatrix}^T$. A transformation that maps $\hat{\boldsymbol{r}}^{(ul)}$ to $\boldsymbol{r}^{(dl)}$ is given by

$$\boldsymbol{r}^{(dl)} = \boldsymbol{\Phi}\hat{\boldsymbol{r}}^{(ul)} + \boldsymbol{\varepsilon}^{(dl)}, \tag{16}$$

where the p,q-th element of $\boldsymbol{\Phi} \in \mathbb{C}^{M \times 2M-1}$ is given by $[\boldsymbol{\Phi}]_{p,q} = \operatorname{sinc}\big(\alpha(p-1) + (M-q)\big)$, $p = 1, \ldots, M$, $q = 1, \ldots, 2M-1$, $\alpha = \frac{f^{(dl)}}{f^{(ul)}}$. Moreover, $\boldsymbol{\varepsilon}^{(dl)} = \begin{bmatrix} \varepsilon_0^{(dl)} & \ldots & \varepsilon_{M-1}^{(dl)} \end{bmatrix}^T$ where

$$|\varepsilon_m^{(dl)}| \leq M\Big(1 - \frac{1}{2\pi}\int_{-\pi}^{\pi} \vartheta(u)\, du\Big) + o(M^{-r}), \tag{17}$$

where $\gamma = \frac{L}{\lambda^{(ul)}}$ and r is the highest continuous derivative of the periodic extension of $\vartheta(\cdot)$, cf. Lemma 1.

Proof: See Appendix B. ∎

From this theorem, it can be seen that for sufficiently small $\|\boldsymbol{\varepsilon}^{(dl)}\|$, we can write

$$\boldsymbol{r}^{(dl)} \approx \boldsymbol{\Phi}\hat{\boldsymbol{r}}^{(ul)}. \tag{18}$$

In particular, whereas the first term of the DCCM estimate, $\boldsymbol{r}^{(dl)}$, in (16) depends only on the UCCM information, i.e., $\hat{\boldsymbol{r}}^{(ul)}$, which is available at the BS, the second term, i.e., $\boldsymbol{\varepsilon}^{(dl)}$, depends on the APS, $\rho(\cdot)$, which is unknown at the BS. This term accounts for the estimation error.

An upper bound on the error incurred by the approximation in (18) is provided in (17). This bound contains two terms. First, we consider the first term. This term arises only for $\gamma > \frac{1}{2}$ and is directly proportional to M, the number of ULA antennas, and the leakage of the transformed APS, i.e., $\rho'(\cdot)$, outside the interval $(-\pi, \pi)$, i.e., $1 - \frac{1}{2\pi}\int_{-\pi}^{\pi} \vartheta(u)\, du$. Therefore, when $\gamma > \frac{1}{2}$, the approximation error corresponding to given number of antennas is smaller for more compact APSs, that is, APSs for which $\frac{1}{2\pi}\int_{-\pi}^{\pi} \vartheta(u) du$ is close to unity. Next, we consider the second term of (17). This term arises for all values of γ, and depends on the number of antennas, M, and the differentiability class, r, of the periodic extension of the transformed APS, $\vartheta(\cdot)$. This term, decreases by increasing M and r. In other words, when $\gamma \leq \frac{1}{2}$, the estimation accuracy of the proposed scheme increases with the number of antennas and the differentiability of the periodic extension of the transformed APS.

Three remarks are in order. First, the proposed scheme yields the exact DCCM when the number of antennas goes to infinity, $\gamma \leq \frac{1}{2}$, and the periodic extension of the transformed APS in (13) is infinitely differentiable, i.e., of class $\mathcal{C}^\infty$. Second, the proposed scheme uses only $2M-1$ out of the M^2 elements of UCCM to compute the DCCM, and third, the entries of the matrix $\boldsymbol{\Phi}$ in (16) are samples of the sinc-function, which depend solely on the ULA antenna-spacing and the ratio of the DL to UL carrier frequencies. Hence, $\boldsymbol{\Phi}$ can be computed offline and stored for future use. These observations guarantee that the proposed scheme not only features superior performance under the aforementioned conditions, but also exhibits a computational complexity that is suitable for practical applications.

B. Proposed Scheme for URA

In this subsection, we propose a novel DCCM estimation scheme for URA systems. Analogous to the scheme proposed for ULA DCCM estimation, this estimation scheme exploits the properties of the URA covariance matrices. These properties are recorded in the following lemma.

Lemma 2: Let $\boldsymbol{R}^{(i)} \in \mathbb{C}^{NM \times NM}$, $i \in \{ul, dl\}$ be the UCCM/DCCM of a URA composed of M antennas in each column and N antennas in each row. The matrix $\boldsymbol{R}^{(i)}$ is a block-Hermitian and block-Toeplitz matrix, that is,

$$\boldsymbol{R}^{(i)} = \begin{bmatrix} \boldsymbol{R}_0^{(i)} & \boldsymbol{R}_{-1}^{(i)} & \cdots & \boldsymbol{R}_{-(N-1)}^{(i)} \\ \boldsymbol{R}_1^{(i)} & \boldsymbol{R}_0^{(i)} & \cdots & \boldsymbol{R}_{-(N-2)}^{(i)} \\ \vdots & \vdots & \cdots & \vdots \\ \boldsymbol{R}_{N-1}^{(i)} & \boldsymbol{R}_{N-2}^{(i)^\dagger} & \cdots & \boldsymbol{R}_0^{(i)} \end{bmatrix}, \quad i \in \{ul, dl\}, \tag{19}$$

with the following properties:

- The main diagonal blocks, i.e., $\boldsymbol{R}_0^{(i)} \in \mathbb{C}^{M \times M}$, are positive semi-definite, Hermitian and Toeplitz with unity diagonal elements.
- The off-diagonal blocks, i.e., $\boldsymbol{R}_n^{(i)} \in \mathbb{C}^{M \times M}$, $n = \pm 1, \ldots, \pm(N-1)$, are Toeplitz.
- The off-diagonal blocks satisfy $\boldsymbol{R}_{-n}^{(i)} = \boldsymbol{R}_n^{(i)^\dagger}$, $n = 1, \ldots, N-1$.

Proof: See Appendix C. ∎

The properties of the UCCM and the DCCM in Lemma 2 will be used to develop the proposed DCCM-estimation scheme. Towards that end, in the following lemma, we will develop a new characterizations of the UCCM and DCCM.

Lemma 3: Let $\boldsymbol{R}^{(i)}$, $i \in \{dl, ul\}$, be the UCCM/DCCM of the channel between a single-antenna user and a BS equipped with a URA in the yz-plane consisting of N L_y-uniformly-spaced antennas in each row and M L_z-uniformly-spaced antennas in each column. Let $\rho(\theta, \phi)$ be the two-dimensional APS where θ and ϕ are the azimuth and elevation AoAs, respectively, and define $\rho'(u, v)$ as follows:

$$\rho'(u,v) = \begin{cases} \frac{\rho(\chi(u,v),\psi(v)) + \rho(\pi - \chi(u,v),\psi(v))}{\sqrt{(a_1^2 - u^2)\big((a_1 a_2)^2 - (a_2 u)^2 - (a_1 v)^2\big)}}, & |u| < \frac{\gamma_y}{\gamma_z}\sqrt{a_2^2 - v^2}, \\ 0 & \text{otherwise}, \end{cases} \tag{20}$$

where

$$\chi(u,v) = 8\pi^3\gamma_y \arcsin\frac{a_2 u}{a_1\sqrt{a_2^2 - v^2}},$$
$$\psi(v) = 8\pi^3\gamma_y \arcsin\frac{v}{a_2}, \tag{21}$$

where $a_1 = 2\pi\gamma_y$, $a_2 = 2\pi\gamma_z$, $\gamma_y = \frac{L_y}{\lambda^{(ul)}}$, and $\gamma_z = \frac{L_z}{\lambda^{(ul)}}$. Moreover, let $\mu^{(ul)}_{n,m}(u,v) = nu + mv$ and $\mu^{(dl)}_{n,m}(u,v) = \alpha\mu^{(ul)}_{n,m}(u,v)$, then the m_1, m_2-th element of the n_1, n_2-th block of $\boldsymbol{R}^{(i)}$, i.e., $[\boldsymbol{R}^{(i)}]_{(n_1,n_2),(m_1,m_2)}$, is given by:

$$[\boldsymbol{R}^{(i)}]_{(n_1,n_2),(m_1,m_2)} = \frac{1}{(2\pi)^2}\int_{-\pi}^{\pi}\int_{-\pi}^{\pi}\vartheta(u,v)e^{\jmath\mu^{(i)}_{n_1-n_2,m_1-m_2}(u,v)}\,du\,dv + \delta^{(i)}_{n_1-n_2,m_1-m_2}, \qquad i\in\{ul,dl\}, \tag{22}$$

where

$$\vartheta(u,v) = \begin{cases}\rho'(u,v), & |u|\le\min(\pi,2\pi\gamma_y),\ |v|\le\min(\pi,2\pi\gamma_z),\\ 0 & \text{otherwise,}\end{cases} \tag{23}$$

and

$$\delta^{(i)}_{n,m} = \frac{1}{(2\pi)^2}\int_{-2\pi\gamma_z}^{2\pi\gamma_z}\int_{-2\pi\gamma_y}^{2\pi\gamma_y}\rho'(u,v)e^{\jmath\mu^{(i)}_{n,m}(u,v)}\,du\,dv - \frac{1}{(2\pi)^2}\int_{-\pi}^{\pi}\int_{-\pi}^{\pi}\vartheta(u,v)e^{\jmath\mu^{(i)}_{n,m}(u,v)}\,du\,dv. \tag{24}$$

Proof: See Appendix D. ∎

The structure of the UCCM and the DCCM in (19) implies that these matrices are completely defined by their first block-column. Furthermore, $\boldsymbol{R}^{(i)}_0$ in this column is itself completely defined by its first column since it is Hermitian and Toeplitz. In contrast, since $\{\boldsymbol{R}^{(i)}_n\}_{n=1}^{N-1}$, are only Toeplitz (cf. Lemma 2), they are completely defined by their first row and first column. Hence, to construct $\boldsymbol{R}^{(i)}$, we use (22) to obtain the elements of the first row and the first column of each block of the first block-column and the first block-row. (For $\boldsymbol{R}^{(i)}_0$, it suffices to obtain the elements of the first column.) In particular,

$$r^{(i)}_{n,m} = [\boldsymbol{R}^{(i)}]_{(n_1,n_2),(m_1,m_2)}\Big|_{\substack{n=n_1-n_2\\ m=m_1-m_2}}, \tag{25}$$
$$n = 0,\pm1,\ldots,\pm(N-1),\ m = 0,\pm1,\ldots,\pm(M-1),$$

that is, the elements $\{r^{(i)}_{n,m}\}$ are obtained from (22) by substituting n and m for $n_1 - n_2$ and $m_1 - m_2$, respectively. Using this notation, $r^{(i)}_{n,m}$ denotes the first-row elements of the $(n+1)$-th block of the first block-column, $n = 0,\ldots,N-1$, $m = -(M-1),\ldots,0$. Moreover, $r^{(i)}_{n,m}$ denotes the first row of the $(1-n)$-th block of the first block-row, $n = -(N-1),\ldots,0$, $m = -(M-1),\ldots,0$. In the following theorem, we will provide a scheme to obtain $\{r^{(dl)}_{n,m}\}$ from $\{r^{(ul)}_{n,m}\}$.

Theorem 2: For an $N\times M$-antenna URA, let the matrix $\hat{\boldsymbol{R}}^{(ul)}\in\mathbb{C}^{2M-1\times 2N-1}$ contain the first row and the first column of each block the first block-column and the first block-row of the UCCM, i.e., $\hat{\boldsymbol{R}}^{(ul)} = \begin{bmatrix}\boldsymbol{r}^{(ul)}_{-(N-1)} & \cdots & \boldsymbol{r}^{(ul)}_{(N-1)}\end{bmatrix}$, where $\boldsymbol{r}^{(ul)}_n = \begin{bmatrix}r^{(ul)}_{n,-(M-1)} & \cdots & r^{(ul)}_{n,(M-1)}\end{bmatrix}^T$. Moreover, let the vector $\boldsymbol{r}^{(dl)}_n\in\mathbb{C}^{2M-1}$, $n = 0,\ldots,N-1$, contain the first row and the first column of the $(n+1)$-th block of the first column-block of the DCCM, i.e., $\boldsymbol{r}^{(dl)}_n = \begin{bmatrix}r^{(ul)}_{n,-(M-1)} & \cdots & r^{(dl)}_{n,0} & \cdots & r^{(dl)}_{n,(M-1)}\end{bmatrix}^T$. A transformation that maps $\hat{\boldsymbol{R}}^{(ul)}$ to $\boldsymbol{r}^{(dl)}_n$ is given by:

$$\boldsymbol{r}^{(dl)}_n = \boldsymbol{\Psi}\hat{\boldsymbol{R}}^{(ul)}\boldsymbol{\phi}_n + \boldsymbol{\varepsilon}^{(dl)}_n, \quad n = 0,\ldots,N-1, \tag{26}$$

where the p,q-th element of $\boldsymbol{\Psi}\in\mathbb{C}^{(2M-1)\times(2M-1)}$ is $[\boldsymbol{\Psi}]_{p,q} = \operatorname{sinc}(-\alpha(M-p)+(M-q))$, $p,q = 1,\ldots,2M-1$, $\boldsymbol{\phi}_n\in\mathbb{C}^{2N-1}$ is given by

$$\boldsymbol{\phi}_n = \begin{bmatrix}\operatorname{sinc}(\alpha n+(N-1)) & \cdots & \operatorname{sinc}(\alpha n) & \cdots & \operatorname{sinc}\big(\alpha n-(N-1)\big)\end{bmatrix}^T. \tag{27}$$

Moreover, $\boldsymbol{\varepsilon}^{(dl)}_n = \begin{bmatrix}\varepsilon^{(dl)}_{n,-(M-1)} & \cdots & \varepsilon^{(dl)}_{n,(M-1)}\end{bmatrix}^T$, $n = 0,\pm1,\ldots,\pm(N-1)$, $m = 0,\pm1,\ldots,\pm(M-1)$, where

$$|\varepsilon^{(dl)}_{n,m}| \le 4MN\Big(1 - \frac{1}{(2\pi)^2}\int_{-\pi}^{\pi}\int_{-\pi}^{\pi}\vartheta(u,v)\,du\,dv\Big) + o\Big(\big(\min(N,M)\big)^{-k}\Big), \tag{28}$$

where $\gamma_y = \frac{L_y}{\lambda^{(ul)}}$, $\gamma_z = \frac{L_z}{\lambda^{(ul)}}$ and k is the highest continuous derivative of the the periodic extension of $\vartheta(\cdot,\cdot)$, cf. Lemma 3.

Proof: See Appendix E ∎

Analogous to Theorem 1, from this theorem it can be seen that, for sufficiently small $\|\boldsymbol{\varepsilon}^{(dl)}_n\|$, we can write

$$\boldsymbol{r}^{(dl)}_n \approx \boldsymbol{\Psi}\hat{\boldsymbol{R}}^{(ul)}\boldsymbol{\phi}_n. \tag{29}$$

In particular, whereas the first term of the DCCM estimate, $\boldsymbol{r}^{(dl)}_n$, in (26) depends only on the UCCM information, i.e., $\hat{\boldsymbol{R}}^{(ul)}$, which is available at the BS, the second term, i.e., ε, depends on the APS, $\rho(\cdot,\cdot)$, which is unknown at the BS. This term accounts for the estimation error.

An upper bound on the error incurred by the approximation in (29) is provided in (28). The first term of this bound arises only when either $\gamma_y > \frac{1}{2}$, $\gamma_z > \frac{1}{2}$, or both. This term is directly proportional to NM, the number of URA antennas, and the leakage of the transformed APS, $\rho'(u,v)$, outside the square, $\big\{(u,v)|u\in(-\pi,\pi), v\in(-\pi,\pi)\big\}$, i.e., $1 - \frac{1}{(2\pi)^2}\int_{-\pi}^{\pi}\int_{-\pi}^{\pi}\vartheta(u,v)\,du\,dv$. Therefore, when at least one of γ_y and γ_z is greater than $\frac{1}{2}$, the approximation error corresponding to a given number of antennas is smaller for more compact APSs, that is, APSs for which $\frac{1}{(2\pi)^2}\int_{-\pi}^{\pi}\int_{-\pi}^{\pi}\vartheta(u,v)\,du\,dv$ is close to unity. Next, we consider the second term of (28). This term arises for all values of γ_y and γ_z, and depends on $\min(N,M)$, and the differentiability class, k, of the periodic extension of the transformed APS, $\vartheta(\cdot,\cdot)$. This term, decreases by increasing $\min(N,M)$ and k. In other words, when $\gamma_y\le\frac{1}{2}$ and $\gamma_z\le\frac{1}{2}$, the estimation accuracy of the proposed scheme increases with $\min(N,M)$ and the differentiability of the periodic extension of the transformed APS.

Analogous to the case of the ULA (Section III-A), for the URA, we have the following remarks. First, the proposed scheme yields the exact DCCM when $\min(N,M)$ goes to infinity, $\gamma_y\le\frac{1}{2}$, $\gamma_z\le\frac{1}{2}$, and the periodic extension

of the transformed APS in (23) is infinitely differentiable, i.e., of class $\mathcal{C}^\infty$. Second, the proposed scheme uses only $(2N-1)(2M-1)$ out of the $(NM)^2$ elements of UCCM to compute the DCCM, and third, the entries of the matrix $\boldsymbol{\Psi}$ and the entries of the vectors $\{\boldsymbol{\phi}_n\}$ in (26) are samples of the sinc-function, which depend solely on the URA antenna-spacing and the ratio of the DL to UL carrier frequencies. Hence, $\boldsymbol{\Phi}$ and $\{\boldsymbol{\phi}_n\}$ can be computed offline and stored for future use. These observations, analogous to the ULA observations (cf. Section III-A), guarantee that the proposed scheme not only features superior performance under the aforementioned conditions, but also exhibits a computational complexity that is suitable for practical applications. An additional insight that can be drawn from this analysis is that, for a URA with a given number of antennas equal to NM, the best configuration that minimizes the upper bound in (28) is the one in which $\min(N, M)$ is maximized. For instance, if the number of antennas is a complete square, it is optimal to place these antennas on a square grid.

IV. Simulation

To evaluate the performance of the proposed schemes, we consider a single-antenna user communicating with a BS equipped with either a ULA or a URA. The UL and DL channels between the user and the BS antenna array are assumed to be frequency-flat with zero-mean unit-variance Gaussian fading coefficients which are independent, and identically distributed (i.i.d) in time domain and correlated in the spatial domain [13], [16].

We compare the performance of the proposed schemes with that of the scheme presented in [13] and [16]. Since these schemes were proposed for ULA systems, we have extended them to URA systems to in order to compare the with the proposed schemes.

A main motivation for DCCM estimation is for the BS to perform beamforming along the principal eigenvector of the estimated DCCM. Hence, to assess the accuracy of the proposed algorithms, it is necessary to assess the deviation of the principal eigenvector of the estimated DCCM from that of the actual one. Towards that end, we define the deviation metric $\mathcal{L}_{\boldsymbol{R}^{(dl)}}(\boldsymbol{v})$ for any unit norm vector $\boldsymbol{v}$ to be given by

$$\mathcal{L}_{\boldsymbol{R}^{(dl)}}(\boldsymbol{v}) = 1 - \frac{\boldsymbol{v}^\dagger \boldsymbol{R}^{(dl)} \boldsymbol{v}}{\Gamma_{\max}^{(dl)}},$$

where $\Gamma_{\max}^{(dl)}$ is the maximum eigenvalue of $\boldsymbol{R}^{(dl)}$. This metric satisfies the inequality $0 \leq \mathcal{L}_{\boldsymbol{R}^{dl}}(\boldsymbol{v}) \leq 1$. The zero lower bound of this inequality is achieved if and only if $\boldsymbol{v}$ is the principal eigenvector of the actual $\boldsymbol{R}^{(dl)}$. Hence, in the numerical results reported in this section, the metric $\mathcal{L}_{\boldsymbol{R}^{(dl)}}(\hat{\boldsymbol{v}}_{\max})$ is plotted versus $\alpha = \frac{f_d}{f_u}$, where $\hat{\boldsymbol{v}}_{\max}$ is the principal eigenvector of the estimated DCCM. As a baseline benchmark, we also present simulation results for the case in which the UCCM observed at the BS is directly used as the DCCM. Next, we outline the main steps used in the simulations.

A. Simulation Steps

1) For M-antenna ULA systems, we generate a random APS $\rho(\theta)$ satisfying $\int_{-\frac{\pi}{2}}^{\frac{\pi}{2}} \rho(\theta) d\theta = 1$. Analogously, for $N \times M$-antenna URA systems, we generate a random APS $\rho(\theta, \phi)$ satisfying $\int_{-\frac{\pi}{2}}^{\frac{\pi}{2}} \int_{-\pi}^{\pi} \rho(\theta, \phi) d\theta d\phi = 1$.
2) Substituting for $\rho(\theta)$ generated in step 1 in (4) yields the $M \times M$ UCCM and DCCM of the M-antenna ULA system. Analogously, substituting for $\rho(\theta, \phi)$ in (6) yields the $NM \times NM$ UCCM and DCCM of the $N \times M$-antenna URA system.
3) Using the UCCMs, $\boldsymbol{R}^{(ul)}$, obtained in step 2, we generate K realizations of the UL channels using

$$\boldsymbol{h}_k^{(ul)} = \boldsymbol{R}^{(ul)^{\frac{1}{2}}} \boldsymbol{h}_k, \qquad k = 1, \ldots, K, \tag{30}$$

where $\boldsymbol{h}_k \in \mathbb{C}^M$ for ULAs and $\boldsymbol{h}_k \in \mathbb{C}^{NM}$ for URAs is a Gaussian random vector with zero mean and identity covariance matrix. We set $K = 10^4$ throughout.
4) For the BS to estimate the respective UCCMs, the user sends K unit pilots causing the signal received at the BS to be represented by:

$$\hat{\boldsymbol{h}}_k^{(ul)} = \boldsymbol{h}_k^{(ul)} + \boldsymbol{n}_k, \qquad k = 1, \ldots, K, \tag{31}$$

where $\boldsymbol{n}_k \in \mathbb{C}^M$ for ULAs and $\boldsymbol{n}_k \in \mathbb{C}^{NM}$ for URAs is zero-mean Gaussian noise with covariance matrix $\sigma_n^2 \boldsymbol{I}$, where $\boldsymbol{I}$ is the identity matrix. Using this notation, the signal to noise ratio (SNR) can be expressed as $\beta = \frac{\mathrm{tr}(\boldsymbol{R}^{(ul)})}{\sigma_n^2}$. In all simulations, β is set to 35 dB.
5) Using (31), the UCCM observed at the BS can be obtained by

$$\hat{\boldsymbol{R}}^{(ul)} = \frac{1}{K} \sum_{k=1}^{K} \hat{\boldsymbol{h}}_k^{(ul)} \hat{\boldsymbol{h}}_k^{(ul)^\dagger} - \sigma_n^2 \boldsymbol{I}. \tag{32}$$

6) For the case of the ULA systems, the UCCM $\boldsymbol{R}^{(ul)}$ obtained in step 1 is Hermitian, positive semi-definite and Toeplitz (cf. Section II-A). However, the UCCM observed at the BS, $\hat{\boldsymbol{R}}^{(ul)}$ in (32), may not necessarily possess these properties. To impose them, we project $\hat{\boldsymbol{R}}^{(ul)}$ on the cone of Toeplitz, positive semi-definite and Hermitian $M \times M$ matrices denoted by $\mathcal{T}_+^M$. Given $\hat{\boldsymbol{R}}^{(ul)}$ in (32), this projection can be described as the following convex optimization [13], [16]:

$$\tilde{\boldsymbol{R}}^{(ul)} = \arg\min_{\mathcal{T}_+^M} \|\boldsymbol{X} - \hat{\boldsymbol{R}}^{(ul)}\|^2. \tag{33}$$

For the case of the URA systems, we consider a block-Toeplitz structure for the UCCM $\hat{\boldsymbol{R}}^{(ul)}$ in (32) analogous to the one in (19). In particular, considering the first block-column, we denote the first block by $\hat{\boldsymbol{R}}_0^{(ul)}$ and we denote the other blocks by $\hat{\boldsymbol{R}}_n^{(ul)}$, $n = 1, \ldots, N-1$, where each block $\{\hat{\boldsymbol{R}}_n^{(ul)}\}_{n=0}^{N-1}$ is an $M \times M$ matrix. The UCCM obtained in step 1, for URA systems, is block-Toeplitz where diagonal blocks are Hermitian, positive semi-definite and Toeplitz while off-diagonal blocks are only Toeplitz (cf. Lemma 2). As in the ULA case, these properties may not hold for the UCCM in (32). To impose this structure, for the diagonal blocks, we use the projection in (33) wherein $\hat{\boldsymbol{R}}^{(ul)}$ is replaced

by $\hat{\boldsymbol{R}}_0^{(ul)}$ and $\tilde{\boldsymbol{R}}^{(ul)}$ is replaced by $\tilde{\boldsymbol{R}}_0^{(ul)}$. For the off-diagonal blocks, we project each block on the cone of $M \times M$ complex Toeplitz matrices denoted by $\mathcal{T}^M$. This projection can be described by the following convex optimization:

$$\tilde{\boldsymbol{R}}_n^{(ul)} = \arg\min_{\mathcal{T}^M} \|\boldsymbol{X}_n - \hat{\boldsymbol{R}}_n^{(ul)}\|^2, \ n = 1, \ldots, N-1. \tag{34}$$

Using $\{\tilde{\boldsymbol{R}}_n^{(ul)}\}_{n=0}^{N-1}$, we construct $\tilde{\boldsymbol{R}}^{(ul)}$, cf. (19).

7) The ULA and URA UCCMs obtained in step 6 are used in (18) and (29) to estimate the respective DCCMs.

B. ULA Simulation Results

In this section we compare the results obtained using the scheme proposed herein for a BS equipped with an M-antenna ULA with the schemes proposed in [23] and [16].

We note that, the scheme in [23] considers an angular range limited to $[-\frac{\pi}{2}, \frac{\pi}{2})$ whereas the scheme proposed herein and the one proposed in [16] consider the angular range $[-\pi, \pi)$. For fair comparison, we will consider APSs that span the range $[-\frac{\pi}{2}, \frac{\pi}{2})$. Moreover, in implementing the scheme in [23], the grid size used in APS estimation is set to $4M$ [23].

Example 1: In this example, we consider a ULA with 64 antennas and a deterministic weighted Gaussian APS given by

$$\rho(\theta) = \frac{w}{\sqrt{2\pi}\sigma_\theta} e^{-\frac{(\theta - m_\theta)^2}{2\sigma_\theta^2}}, \tag{35}$$

where the mean, m_θ, and the standard deviation, σ_θ, are uniformly drawn form $[-\frac{\pi}{3}, \frac{\pi}{3}]$ and $[\frac{\pi}{60}, \frac{\pi}{20}]$, respectively [16], and w is chosen to ensure that $\int_{-\frac{\pi}{2}}^{\frac{\pi}{2}} \rho(\theta)\, d\theta = 1$. The performance of the scheme proposed herein and that of the ones proposed in [23] and [16] are depicted versus $\alpha = \frac{f_d}{f_u}$ in Figures 3, 4 and 5, for $\gamma = 0.3$, $\gamma = 0.5$, and $\gamma = 0.7$, respectively. These figures include the baseline where the observed UCCM at the BS is used directly as the estimated DCCM.

Figure 3 shows that, for $\gamma = 0.3$, the scheme proposed herein and the ones in [16] and [23] significantly outperform the baseline. In particular, all three schemes experience close performance for $\alpha \leq 1.1$. However, for $\alpha > 1.1$, the proposed scheme outperforms the other ones. For instance, at $\alpha = 1.2$, the proposed scheme exhibits a deviation metric of 6.5×10^{-4}, whereas the schemes proposed in [16] and [23] exhibit deviation metrics of 1.2×10^{-3} and 5×10^{-3}, respectively.

Similar to Figure 3, Figure 4 shows that, for $\gamma = 0.5$, all three schemes outperform the baseline. In particular, the scheme proposed herein and the one proposed in [16] provide almost the same performance for all values of α and both outperform the scheme proposed in [23], specially for $\alpha > 1.06$. For instance, at $\alpha = 1.2$, our scheme and the one in [16] exhibit a deviation metric of 1.5×10^{-3} whereas the scheme in [23] exhibits a deviation metric of 5.5×10^{-3}. A similar phenomenon is observed for the scheme proposed in [16].

Finally, for $\gamma = 0.7$, Figure 5 shows that the scheme proposed herein significantly outperforms the ones proposed in [23] and [16] for all values of α. In fact, for any $\gamma > 0.5$, the scheme proposed in [23] is unable to recover the APS samples due to aliasing [23]. □

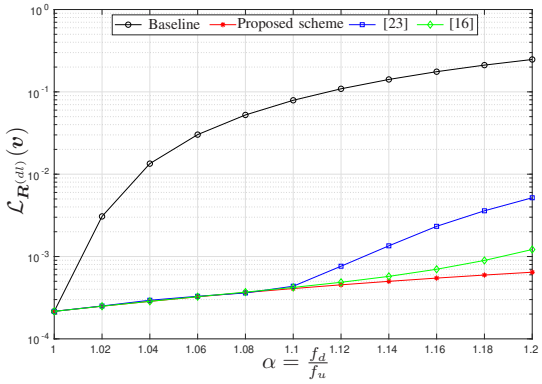

Fig. 3: Performance of the proposed scheme, [23], and [16] for a 64-antenna ULA when $\gamma = 0.3$.

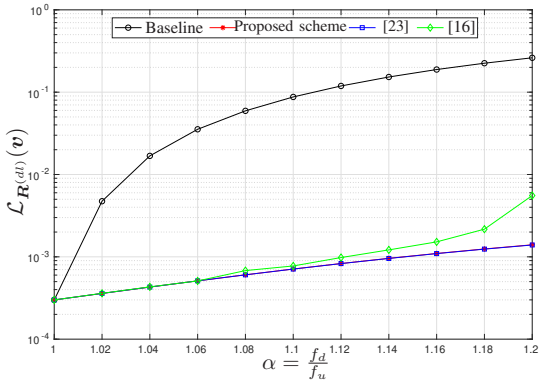

Fig. 4: Performance of the proposed scheme, [23], and [16] for a 64-antenna ULA when $\gamma = 0.5$.

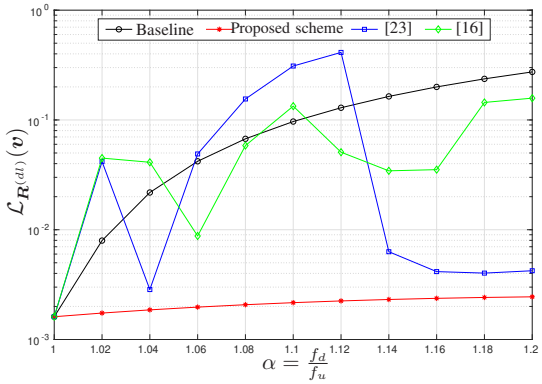

Fig. 5: Performance of the proposed scheme, [23], and [16] for a 64-antenna ULA when $\gamma = 0.7$.

C. URA Simulation Results

In this section, we present the results obtained for a BS equipped with an $N \times M$-antenna URA URA. For comparison purposes, we extended the scheme proposed in [23] for ULAs to the URAs considered herein.

Example 2: In this example, we consider a URA with 64×64 antennas and a deterministic two-dimensional truncated normalized Gaussian-shaped APSs that is, $\rho(\theta, \phi) = \rho_1(\theta)\rho_2(\phi)$, where $\rho_i(\cdot) = \rho(\cdot)$ are given in (35), $i = 1, 2$, with distinct means, variances and normalization factors. This choice of the APSs ensures that $\int_{-\pi}^{\pi} \int_{-\frac{\pi}{2}}^{\frac{\pi}{2}} \rho(\theta, \phi)\, d\theta\, d\phi = 1$. The means and variances, m_θ and σ_θ, are uniformly drawn from $[-\frac{\pi}{6}, \frac{\pi}{6}]$ and $[\frac{\pi}{45}, \frac{\pi}{20}]$, respectively, while the means and variances, m_ϕ and σ_ϕ, are uniformly drawn from $[-\frac{\pi}{4}, \frac{\pi}{4}]$ and $[\frac{\pi}{180}, \frac{\pi}{20}]$, respectively [20].

The performance of the scheme proposed herein and that of the extended version of the one proposed in [23] are depicted versus α in Figures 6, 7 and 8, for $\gamma_y = \gamma_z = 0.3$, $\gamma_y = \gamma_z = 0.5$, and $\gamma_y = \gamma_z = 0.7$, respectively. Similar to Example 1, these figures include the baseline as a benchmark.

Figures 6 and 7 show that, for $\gamma_y = \gamma_z = 0.3$ and $\gamma_y = \gamma_z = 0.5$, the scheme proposed herein and the extended version of the one proposed in [23] significantly outperform the baseline. Moreover, the proposed scheme outperforms the extended version of the scheme proposed in [23] specially for $\alpha > 1.1$. For instance, at $\alpha = 1.2$ and $\gamma_y = \gamma_z = 0.5$, the proposed scheme exhibits a deviation metric of 2×10^{-3}, whereas the extended version of the scheme proposed in [23] exhibits a deviation metric of 1×10^{-2}. These observations mirror the ULA case in Example 1.

Figure 8 shows that, for $\gamma_y = \gamma_z = 0.7$, the scheme proposed herein significantly outperforms the extended version of the one proposed in [23] for all values of α. For instance, it can be seen that the baseline scheme performs slightly better than the extended version of the scheme proposed in [23]. This is due to the fact that the extended version of the scheme proposed in [23] cannot recover the APS samples due to aliasing when either γ_y, γ_z or both are greater than 0.5. This is in line with the observations for the case of ULA seen in Example 1. Moreover, it can be seen from Figures 6, 7 and 8 that our scheme exhibits low sensitivity to the changes in α in contrast with the extended version of [23], which is highly sensitive to these changes. □

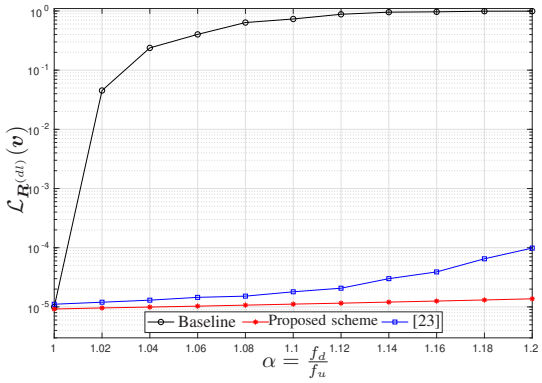

Fig. 6: Performance of the proposed scheme and [23] for a 64×64-antenna URA when $\gamma_y = \gamma_z = 0.3$.

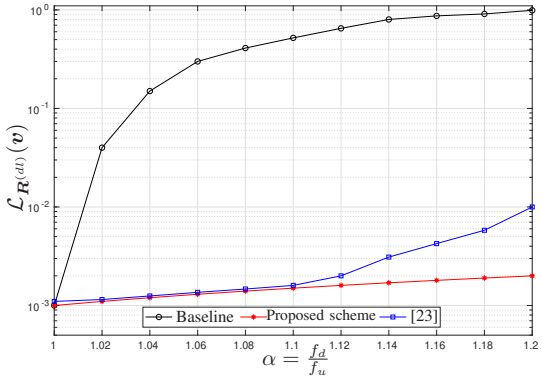

Fig. 7: Performance of the proposed scheme and [23] for 64×64-antenna when $\gamma_y = \gamma_z = 0.5$.

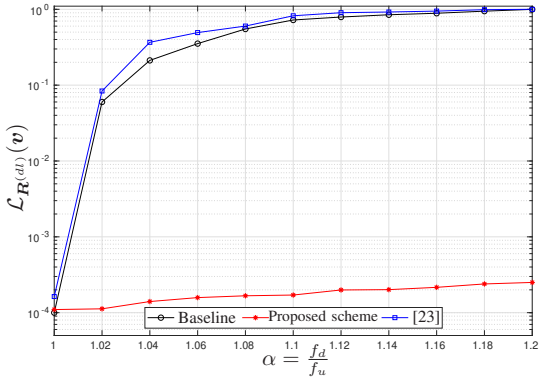

Fig. 8: Performance of the proposed scheme and [23] for 64×64-antenna when $\gamma_y = \gamma_z = 0.7$.

V. Conclusion

This paper proposed DCCM estimation schemes for FDD mMIMO systems in which the BS is equipped with either a ULA or a URA. The proposed DCCM estimation schemes have three attractive features: first, they can be represented as affine transformations of the UCCM that depend only on the array geometry and carrier frequencies; hence, they can be computed offline. Second, they use few elements of the UCCM observed at the BS; hence, they have low computational complexity. Third, they exhibit low sensitivity to changes in UL/DL carrier separation compared to other schemes proposed in the literature. Upper bounds on the estimation error of the proposed schemes were derived. These bounds showed

that, first, the accuracy of the proposed schemes increases with the number of ULA/URA antennas, the compactness and differentiability class of the periodic extension of the transformed APS. In particular, for an infinite number of antennas, under certain condition of compactness and differentiability, the estimated DCCMs will be equal to the true DCCMs. Numerical simulations confirm the performance superiority of the proposed schemes over their existing counterparts.

APPENDIX A
PROOF OF LEMMA 1

Setting $i = ul$ in (5), we can write

$$[\boldsymbol{R}^{(ul)}]_{p,q} = \int_{-\pi}^{\pi} \rho(\theta) e^{\jmath 2\pi(p-q)\gamma \sin(\theta)} \mathrm{d}\theta \tag{36}$$

$$= \int_{-\frac{\pi}{2}}^{\frac{\pi}{2}} \rho_1(\theta) e^{\jmath 2\pi(p-q)\gamma \sin(\theta)} \mathrm{d}\theta, \quad \rho_1(\theta) = \rho(\theta) + \rho(\pi - \theta) \tag{37}$$

$$= \int_{-1}^{1} \rho_2(t) e^{\jmath 2\pi(p-q)\gamma t} \mathrm{d}t, \ \rho_2(t) = \frac{\rho_1(\arcsin(t))}{\sqrt{1-t^2}}, \ t = \sin(\theta)$$

$$= \frac{1}{2\pi} \int_{-2\pi\gamma}^{2\pi\gamma} \rho'(u) e^{\jmath(p-q)u} \mathrm{d}u, \ \rho'(u) = \frac{\rho_2\left(\frac{u}{2\pi\gamma}\right)}{\gamma}, \ u = 2\pi\gamma t \tag{38}$$

Equation (37) results from the fact that both $\rho(\theta)$ and $\exp((p-q)\gamma \sin(\theta))$ in (36) are periodic with period of 2π. In particular, changing the limits of integration to $-\frac{\pi}{2}$ and $\frac{3\pi}{2}$ and, writing the integral as $\int_{-\frac{\pi}{2}}^{\frac{\pi}{2}} \rho(\theta) e^{\jmath 2\pi(p-q)\frac{d}{\lambda_u}\sin(\theta)} \mathrm{d}\theta + \int_{\frac{\pi}{2}}^{\frac{3\pi}{2}} \rho(\theta) e^{\jmath 2\pi(p-q)\frac{d}{\lambda_u}\sin(\theta)} \mathrm{d}\theta$, and finally, using the following change of variables in the second integral: $\theta_1 = \pi - \theta$ yields (37). Analogously, following similar steps yields that the pq-th DDCM element is given by

$$[\boldsymbol{R}^{(dl)}]_{p,q} = \frac{1}{2\pi} \int_{-2\pi\gamma}^{2\pi\gamma} \rho'(u) e^{\jmath(p-q)\alpha u} du. \tag{39}$$

Using (38) and (39), we can write

$$[\boldsymbol{R}^{(i)}]_{p,q} = \frac{1}{2\pi} \int_{-2\pi\gamma}^{2\pi\gamma} \rho'(u) e^{\jmath \mu_{p,q}^{(i)}(u)} du, \quad i \in \{ul, dl\},$$
$$\rho'(u) = \frac{\rho(\arcsin\frac{u}{2\pi\gamma}) + \rho(\pi - \arcsin\frac{u}{2\pi\gamma})}{\sqrt{\gamma^2 - (\frac{u}{2\pi})^2}}, \tag{40}$$

where

$$\mu_{p,q}^{(i)}(u) = \begin{cases} (p-q)u & i = ul, \\ (p-q)\alpha u & i = dl. \end{cases}$$

Using $\vartheta(u)$ defined in (13), we can rewrite (40) as (12), which completes the proof.

APPENDIX B
PROOF OF THEOREM 1

We consider a periodic extension of the transformed APS, $\vartheta(\cdot)$, which we refer to as $\vartheta'(\cdot)$. In particular, for any $u \in (-\pi, \pi)$, we assume that

$$\vartheta'(u) = \vartheta'(u + 2n\pi) = \vartheta(u), \qquad n = \pm 1, \pm 2, \ldots. \tag{41}$$

The Fourier series expansion of $\vartheta'(\cdot)$ is given by

$$\vartheta'(u) = \sum_{m=-\infty}^{\infty} c_m e^{-\jmath m u}, \tag{42}$$

where the coefficients $\{c_m\}$ are given by

$$c_m = \frac{1}{2\pi} \int_{2\pi} \vartheta'(u) e^{\jmath m u} du. \tag{43}$$

Comparing the Fourier series coefficients c_m in (43) with $r_m^{(i)}$, $i = ul$ in (15) and invoking the definition of $\vartheta'(\cdot)$ in (41), it can be readily shown that

$$r_m^{(ul)} = c_m + \delta_m^{(ul)}, \qquad m = 0, \pm 1, \ldots, \pm(M-1). \tag{44}$$

Substituting for $\{c_m\}_{m=-(M-1)}^{M-1}$ from (44) in (42), we have

$$\begin{aligned} \vartheta'(u) &= \sum_{m=-M+1}^{M-1} c_m e^{-\jmath m u} + \sum_{|m|\geq M} c_m e^{-\jmath m u} \\ &= \sum_{m=-M+1}^{M-1} r_m^{(ul)} e^{-\jmath m u} - \sum_{m=-M+1}^{M-1} \delta_m^{(ul)} e^{-\jmath m u} \\ &\quad + \sum_{|m|\geq M} c_m e^{-\jmath m u}. \end{aligned} \tag{45}$$

Using (41), we can substitute for $\vartheta(u)$ from (45) in (15) with $i = dl$, which yields

$$\begin{aligned} r_m^{(dl)} &= \frac{1}{2\pi} \int_{-\pi}^{\pi} \Big(\sum_{k=-M+1}^{M-1} r_k^{(ul)} e^{-\jmath k u} \Big) e^{\jmath \alpha m u} du \\ &\quad - \frac{1}{2\pi} \int_{-\pi}^{\pi} \Big(\sum_{k=-M+1}^{M-1} \delta_k^{(ul)} e^{-\jmath k u} \Big) e^{\jmath \alpha m u} du \\ &\quad + \frac{1}{2\pi} \int_{-\pi}^{\pi} \Big(\sum_{|k|\geq M} c_k e^{-\jmath k u} \Big) e^{\jmath \alpha m u} du + \delta_m^{(dl)} \end{aligned} \tag{46}$$

$$= \sum_{k=-M+1}^{M-1} r_k^{(ul)} \operatorname{sinc}(\alpha m - k) + \varepsilon_m^{(dl)}, \tag{47}$$

where

$$\begin{aligned} \varepsilon_m^{(dl)} &= - \sum_{k=-M+1}^{M-1} \delta_k^{(ul)} \operatorname{sinc}(\alpha m - k) \\ &\quad + \sum_{|k|\geq M} c_k \operatorname{sinc}(\alpha m - k) + \delta_m^{(dl)}. \end{aligned} \tag{48}$$

To obtain (47) and (48), we switched the order of summation and integral and used $\frac{1}{2\pi}\int_{-\pi}^{\pi} e^{\jmath k u} du = \operatorname{sinc}(k)$ in the first three terms on the RHS of (46). We can rewrite (47) in the following matrix format

$$\boldsymbol{r}^{(dl)} = \boldsymbol{\Phi} \hat{\boldsymbol{r}}^{(ul)} + \boldsymbol{\varepsilon}^{(dl)}, \tag{49}$$

where $\boldsymbol{r}^{(dl)}$, $\boldsymbol{\Phi}$ and $\hat{\boldsymbol{r}}^{(ul)}$ are given in Theorem 1 and $\boldsymbol{\varepsilon}^{(dl)} = \begin{bmatrix} \varepsilon_0^{(dl)} & \cdots & \varepsilon_{M-1}^{(dl)} \end{bmatrix}^T$. An upper bound on $|\varepsilon_m^{(dl)}|$, $m = 0, \cdots, (M-1)$, is provided in the following lemma. This lemma along with (49) completes the proof.

Lemma 4: $|\varepsilon_m^{(dl)}|$ is upper bounded by

$$|\varepsilon_m^{(dl)}| \leq 2M \Big(1 - \frac{1}{2\pi} \int_{-\pi}^{\pi} \vartheta(u) du \Big) + o(M^{-r}). \tag{50}$$

Proof: Using the fact that $|\operatorname{sinc}(\cdot)| \leq 1$ in (48) yields:

$$|\varepsilon_m^{(dl)}| \leq \sum_{k=-(M-1)}^{(M-1)} |\delta_k^{(ul)}| + \sum_{|k|\geq M} |c_k| + |\delta_m^{(dl)}|. \quad (51)$$

First, we consider the first and third terms on the RHS of (51). Using (14), it can be shown that

$$\begin{aligned}\delta_m^{(i)} &= \frac{1}{2\pi}\int_{-2\pi\gamma}^{2\pi\gamma} \rho'(u) e^{\jmath\mu_m^{(i)}}\, du \\ &\quad - \frac{1}{2\pi}\int_{-\min(\pi,2\pi\gamma)}^{\min(\pi,2\pi\gamma)} \rho'(u) e^{\jmath\mu_m^{(i)}}\, du \\ &= \frac{1}{2\pi}\int_{\mathcal{A}_1\setminus\mathcal{A}_2} \rho'(u) e^{\jmath\mu_m^{(i)}}\, du, \end{aligned} \quad (52)$$

where $\mathcal{A}_1 = \Big\{u \big| |u| \leq 2\pi\gamma\Big\}$ and $\mathcal{A}_2 = \Big\{u \big| |u| \leq \min(\pi, 2\pi\gamma)\Big\}$. Using (52) along with the definition of $\vartheta(\cdot)$ in (13), we can write

$$\begin{aligned}|\delta_m^{(i)}| &\leq \frac{1}{2\pi}\int_{-2\pi\gamma}^{2\pi\gamma} \rho'(u)\, du - \frac{1}{2\pi}\int_{-\min(\pi,2\pi\gamma)}^{\min(\pi,2\pi\gamma)} \rho'(u)\, du \\ &= 1 - \frac{1}{2\pi}\int_{-\pi}^{\pi} \vartheta(u)\, du. \end{aligned} \quad (53)$$

To obtain (53), we used the fact that the APS $\rho(\theta)$ is a real, positive function satisfying $\int_{-\pi}^{\pi} \rho(\theta)\, d\theta = 1$ and hence, $\rho'(u)$ in (40) is also real, positive satisfying $\frac{1}{2\pi}\int_{-2\pi\gamma}^{2\pi\gamma} \rho'(\theta) d\theta = 1$.

So far, we have obtained an upper bound on the first and third terms on the RHS of (51). Now, we consider the second term on the RHS of (51). To obtain an upper bound on that term, we use the fact that, for a $\mathcal{C}^r$-periodic function $f(x)$, i.e., $f(x)$ has r continuous derivatives, the m-th Fourier series coefficient decays faster than $\frac{1}{m^r}$, that is, $|c_m| = o(\frac{1}{m^r})$. Assuming that $\vartheta'(u)$ belongs to $\mathcal{C}^r$, we can write

$$\begin{aligned}\sum_{|k|\geq M} |c_k| &= \sum_{|k|\geq M} o(k^{-r}) \\ &= o(M^{-r}), \end{aligned} \quad (54)$$

To obtain (54), we used the fact that if $|c_{K+i}| = o\big((k+i)^{-r}\big)$ then we have $|c_{K+i}| = o\big(k^{-r}\big)$. Using (53) and (54) in (51) yields the bound in (50), and completes the proof of Lemma 4. ∎

Appendix C
Proof of Lemma 2

To prove this lemma, we begin by considering the matrix $\boldsymbol{A}^{(i)} = \boldsymbol{a}^{(i)}(\theta,\phi)\boldsymbol{a}^{(i)^\dagger}(\theta,\phi) \in \mathbb{C}^{NM\times NM}$, $\boldsymbol{R}^{(i)}$. Using (7), it can be readily verified that $\boldsymbol{A}^{(i)}$ has the following structure[1]:

$$\boldsymbol{A}^{(i)} = \begin{bmatrix} \boldsymbol{a}_1^{(i)}\boldsymbol{a}_1^{(i)^\dagger} & \cdots & \boldsymbol{a}_1^{(i)}\boldsymbol{a}_N^{(i)^\dagger} \\ \vdots & \ddots & \vdots \\ \boldsymbol{a}_N^{(i)}\boldsymbol{a}_1^{(N)^\dagger} & \cdots & \boldsymbol{a}_N^{(i)}\boldsymbol{a}_N^{(i)^\dagger} \end{bmatrix}, \quad i \in \{ul, dl\}. \quad (55)$$

[1]For notational convenience, the dependence on the (θ,ϕ) has been dropped in this appendix.

Using (8) and (9), each block $\boldsymbol{a}_{n_1}^{(i)}\boldsymbol{a}_{n_2}^{(i)^\dagger} \in \mathbb{C}^{M\times M}$, $n_1, n_2 = 1,\ldots,N$, can be expressed by

$$\boldsymbol{a}_{n_1}^{(i)}\boldsymbol{a}_{n_2}^{(i)^\dagger} = \nu \begin{bmatrix} 1 & e^{-\jmath g(\phi)} & \cdots & e^{-\jmath(M-1)g(\phi)} \\ \vdots & \vdots & \ddots & \vdots \\ e^{\jmath(M-1)g(\phi)} & e^{\jmath(M-2)g(\phi)} & \cdots & 1 \end{bmatrix}, \quad (56)$$

where $\nu = e^{\jmath\frac{2\pi}{\lambda^{(i)}}(n_1-n_2)L_y\sin(\theta)\cos(\phi)}$ and $g(\phi) = \frac{2\pi}{\lambda^{(i)}}L_z\sin(\phi)$. Using (56), it can be seen that:

- $\boldsymbol{a}_{n_1}^{(i)}\boldsymbol{a}_{n_1}^{(i)^\dagger} = \boldsymbol{a}_{n_2}^{(i)}\boldsymbol{a}_{n_2}^{(i)^\dagger}, \forall n_1, \forall n_2$, that is, the main-diagonal blocks of $\boldsymbol{A}^{(i)}$ are equal;
- $\boldsymbol{a}_{n_1}^{(i)}\boldsymbol{a}_{n_2}^{(i)^\dagger} = \boldsymbol{a}_{n_1+1}^{(i)}\boldsymbol{a}_{n_2+1}^{(i)^\dagger}$, $n_1, n_2 = 1,\ldots,N-1$, i.e., non-principal diagonal blocks are equal;
- each diagonal block $\boldsymbol{a}_{n_1}^{(i)}\boldsymbol{a}_{n_1}^{(i)^\dagger}$, $\forall n_1$, is positive semi-definite, Hermitian and Toeplitz with diagonal elements equal to 1; and,
- off-diagonal blocks $\boldsymbol{a}_{n_1}^{(i)}\boldsymbol{a}_{n_2}^{(i)^\dagger}$, $n_1 \neq n_2$, are only Toeplitz.

Combining these properties yields that the matrix $\boldsymbol{A}^{(i)}$, $i \in \{ul, dl\}$, is block-Hermitian (subsequently Hermitian) and block-Toeplitz. Using the fact that $\rho(\theta,\phi)$ is real and positive for all θ and ϕ, it follows that the matrix $\boldsymbol{R}^{(i)}$ defined in (6) possesses the same properties as $\boldsymbol{A}^{(i)}$, $i \in \{ul, dl\}$.

Appendix D
Proof of Lemma 3

Using (10) with $i = ul$, $\gamma_y = \frac{L_y}{\lambda^{(ul)}}$, and $\gamma_z = \frac{L_z}{\lambda^{(ul)}}$, it can be shown that the m_1m_2-th element of the n_1n_2-th block of $\boldsymbol{R}^{(ul)}$, i.e., $[\boldsymbol{R}^{(ul)}]_{(n_1,n_2),(m_1,m_2)}$, is given by:

$$\begin{aligned}&[\boldsymbol{R}^{(ul)}]_{(n_1,n_2),(m_1,m_2)} \\ &= \int_{-\frac{\pi}{2}}^{\frac{\pi}{2}}\int_{-\pi}^{\pi} \rho(\theta,\phi) e^{\jmath\frac{2\pi}{\lambda^{(ul)}}D_{n_1n_2m_1m_2}(\theta,\phi)}\, d\theta\, d\phi \\ &= \int_{-\frac{\pi}{2}}^{\frac{\pi}{2}}\int_{-\frac{\pi}{2}}^{\frac{\pi}{2}} \rho_1(\theta,\phi) e^{\jmath\frac{2\pi}{\lambda^{(ul)}}D_{n_1n_2m_1m_2}(\theta,\phi)}\, d\theta\, d\phi \quad (57) \\ &= \int_{-1}^{1}\int_{-\sqrt{1-z^2}}^{\sqrt{1-z^2}} \rho_2(y,z) e^{\jmath\frac{2\pi}{\lambda^{(ul)}}\left((n_1-n_2)L_y y + (m_1-m_2)L_z z\right)}\, dy\, dz \quad (58) \\ &= \int_{-1}^{1}\int_{-1}^{1} \rho_3(y,z) e^{\jmath 2\pi\left(\gamma_y(n_1-n_2)y + \gamma_z(m_1-m_2)z\right)}\, dy\, dz \quad (59) \\ &= \frac{1}{(2\pi)^2}\int_{-2\pi\gamma_z}^{2\pi\gamma_z}\int_{-2\pi\gamma_y}^{2\pi\gamma_y} \rho'(u,v) e^{\jmath\left((n_1-n_2)u + (m_1-m_2)v\right)}\, du\, dv, \quad (60) \end{aligned}$$

where $D_{n_1n_2m_1m_2}(\theta,\phi)$ is given in (10) and

$$\begin{aligned}\rho_1(\theta,\phi) &= \rho(\theta,\phi) + \rho(\pi-\theta,\phi), \\ \rho_2(y,z) &= \frac{\rho_1(\arcsin\frac{y}{\sqrt{1-z^2}}, \arcsin z)}{\sqrt{(1-y^2)(1-y^2-z^2)}}, \\ &\qquad y = \sin(\theta)\cos(\phi),\ z = \sin(\phi), \\ \rho_3(y,z) &= \begin{cases} \rho_2(y,z), & |y| < \sqrt{1-z^2}, \\ 0, & \text{otherwise}, \end{cases} \end{aligned}$$

$$\rho'(u,v)=\frac{1}{\gamma_y\gamma_z}\rho_3\big(\frac{u}{2\pi\gamma_y},\frac{v}{2\pi\gamma_z}\big),\ u=2\pi\gamma_y y,\ v=2\pi\gamma_z z. \tag{61}$$

Following steps analogous to those used to obtain (37) yields (57). To obtain (58), we used the change of variables: $z=\sin(\phi)$ and $y=\sin(\theta)\cos(\phi)$ To obtain (59), we used $\rho_3(y,z)$ from (61). Finally, to obtain (60), we used the change of variables $u=2\pi\gamma_y y$ and $v=2\pi\gamma_z z$. For the DL case, using (10) and following steps analogous to those used above for the UL yields:

$$[\boldsymbol{R}^{(dl)}]_{(n_1,n_2),(m_1,m_2)}= \frac{1}{(2\pi)^2}\int_{-2\pi\gamma_z}^{2\pi\gamma_z}\int_{-2\pi\gamma_y}^{2\pi\gamma_y}\rho'(u,v)e^{\jmath\alpha\big((n_1-n_2)u+(m_1-m_2)v\big)}dudv. \tag{62}$$

Combining (60) and (62), and defining $\vartheta(\theta,\phi)$ as in (23) yield the statement of the lemma.

Appendix E
Proof of Theorem 2

Analogous to the ULA, we consider a two-dimensional periodic extension of the transformed APS, $\vartheta(\cdot,\cdot)$, which we refer to as $\vartheta'(\cdot,\cdot)$. In particular, for any $u,v\in(-\pi,\pi)$,

$$\vartheta'(u,v)=\vartheta'(u+2n\pi,v+2m\pi)=\vartheta(u,v),\quad n,m=\pm1,\pm2,\ldots. \tag{63}$$

The Fourier series expansion of $\vartheta'(u,v)$ is given by

$$\vartheta'(u,v)=\sum_{n=-\infty}^{\infty}\sum_{m=-\infty}^{\infty}c_{n,m}e^{-\jmath(nu+mv)}, \tag{64}$$

where the coefficients $\{c_{n,m}\}$ are given by [29]

$$c_{n,m}=\frac{1}{(2\pi)^2}\int_{-\pi}^{\pi}\int_{-\pi}^{\pi}\vartheta'(u,v)e^{\jmath(nu+mv)}\,du\,dv. \tag{65}$$

Comparing the Fourier series coefficients $c_{n,m}$ in (65) with $r_{n,m}^{(i)}$, $i=ul$ in (25) and invoking the definition of $\vartheta'(\cdot,\cdot)$ in (63), it can be readily shown that

$$r_{n,m}^{(ul)}=c_{n,m}+\delta_{n,m}^{(ul)},\quad n=0,\pm1,\ldots,\pm(N-1),\ m=0,\pm1,\ldots,\pm(M-1). \tag{66}$$

Letting $\mathcal{S}_{k_1,k_2}=\big\{(n,m)|n=0,\pm1,\ldots,\pm k_1,\ m=0,\pm1,\ldots,\pm k_2\big\}$ and substituting for $\{c_{n,m}\}$, from (66) in (64), we have

$$\vartheta'(u,v)=\sum_{(n,m)\in\mathcal{S}_{N-1,M-1}}(r_{n,m}^{(ul)}-\delta_{n,m}^{(ul)})e^{-\jmath(nu+mv)}+\sum_{(n,m)\in\bar{\mathcal{S}}_{N,M}}c_{n,m}e^{-\jmath(nu+mv)}, \tag{67}$$

where $\bar{\mathcal{S}}_{N,M}=\mathcal{S}_{\infty,\infty}\backslash\mathcal{S}_{N-1,M-1}$. Using (63), we can substitute for $\vartheta(u,v)$ from (67) in (25) with $i=dl$, which yields

$$\begin{aligned}r_{n,m}^{(dl)}&=\frac{1}{(2\pi)^2}\int_{-\pi}^{\pi}\int_{-\pi}^{\pi}\Bigg(\sum_{(n',m')\in\mathcal{S}_{N-1,M-1}}\big(r_{n',m'}^{(ul)}-\delta_{n',m'}^{(ul)}\big)\times e^{-\jmath(n'u+m'v)}\Bigg)e^{\jmath\alpha(nu+mv)}\,du\,dv\\&\quad+\frac{1}{(2\pi)^2}\int_{-\pi}^{\pi}\int_{-\pi}^{\pi}\Bigg(\sum_{(n',m')\in\bar{\mathcal{S}}_{N,M}}c_{n',m'}\times e^{-\jmath(n'u+m'v)}\Bigg)e^{\jmath\alpha(nu+mv)}\,du\,dv+\delta_{n,m}^{(dl)} \qquad (68)\\&=\sum_{(n',m')\in\mathcal{S}_{N-1,M-1}}r_{n',m'}^{(ul)}\operatorname{sinc}(\alpha n-n')\operatorname{sinc}(\alpha m-m')+\varepsilon_{n,m}^{(dl)}, \qquad (69)\end{aligned}$$

where

$$\begin{aligned}\varepsilon_{n,m}^{(dl)}&=\sum_{(n',m')\in\bar{\mathcal{S}}_{N,M}}c_{n',m'}\operatorname{sinc}(\alpha n-n')\operatorname{sinc}(\alpha m-m')\\&\quad-\sum_{(n',m')\in\mathcal{S}_{N-1,M-1}}\delta_{n',m'}^{(ul)}\operatorname{sinc}(\alpha n-n')\operatorname{sinc}(\alpha m-m')+\delta_{n,m}^{(dl)}, \qquad (70)\end{aligned}$$

We can rewrite (69) in the following matrix format

$$\boldsymbol{r}_n^{(dl)}=\boldsymbol{\Psi}\hat{\boldsymbol{R}}^{(ul)}\boldsymbol{\phi}_n+\boldsymbol{\varepsilon}_n^{(dl)},\quad n=0,\ldots,N-1, \tag{71}$$

where $\boldsymbol{r}_n^{(dl)}$, $\boldsymbol{\Psi}$, $\hat{\boldsymbol{R}}^{(ul)}$, and $\boldsymbol{\phi}_n$ are given in Theorem 2 and $\boldsymbol{\varepsilon}_n^{(dl)}=\begin{bmatrix}\varepsilon_{n,-(M-1)}^{(dl)} & \cdots & \varepsilon_{n,(M-1)}^{(dl)}\end{bmatrix}^T$. An upper bound on $\{|\varepsilon_{n,m}^{(dl)}|\}$ is provided in the following lemma. This lemma along with (71) completes the proof.

Lemma 5: $|\varepsilon_{n,m}^{(dl)}|$ is upper bounded by

$$|\varepsilon_{n,m}^{(dl)}|\le 4MN\Big(1-\frac{1}{(2\pi)^2}\int_{-\pi}^{\pi}\int_{-\pi}^{\pi}\vartheta(u,v)\,du\,dv\Big)+o\Big(\big(\min(N,M)\big)^{-k}\Big). \tag{72}$$

Proof: Using the fact that $|\operatorname{sinc}(\cdot)|\le1$ in (70) yields

$$|\varepsilon_{n,m}^{(dl)}|\le\sum_{(n',m')\in\mathcal{S}_{N-1,M-1}}|\delta_{n',m'}^{(ul)}|+\sum_{(n',m')\in\bar{\mathcal{S}}_{N,M}}|c_{n',m'}|+|\delta_{n,m}^{(dl)}|. \tag{73}$$

First, we consider the first and third terms on the RHS of (73). Using (23) and (24), it can be shown that $\delta_{n,m}^{(i)}=\frac{1}{(2\pi)^2}\iint_{\mathcal{A}_1\backslash\mathcal{A}_2}\rho'(u,v)e^{\jmath\mu_{n,m}(u,v)}\,du\,dv$, where $\mathcal{A}_1=\Big\{(u,v)\big||u|\le2\pi\gamma_y,\ |v|\le2\pi\gamma_z\Big\}$ and $\mathcal{A}_2=\Big\{(u,v)\big||u|\le\min(\pi,2\pi\gamma_y),\ |v|\le\min(\pi,2\pi\gamma_z)\Big\}$. Using this along with the definition of $\vartheta(\cdot,\cdot)$ in (23), we can write

$$\begin{aligned}|\delta_{n,m}^{(i)}|&\le\frac{1}{(2\pi)^2}\iint_{\mathcal{A}_1\backslash\mathcal{A}_2}|\rho'(u,v)|\,du\,dv\\&=\frac{1}{(2\pi)^2}\iint_{\mathcal{A}_1}\rho'(u,v)\,du\,dv-\frac{1}{(2\pi)^2}\iint_{\mathcal{A}_2}\rho'(u,v)\,du\,dv\\&=1-\frac{1}{(2\pi)^2}\int_{-\pi}^{\pi}\int_{-\pi}^{\pi}\vartheta(u,v)\,du\,dv. \qquad (74)\end{aligned}$$

To obtain (74), we used the fact that the APS, $\rho(\cdot,\cdot)$, is a real, positive function satisfying $\int_{-\pi}^{\pi}\int_{-\frac{\pi}{2}}^{\frac{\pi}{2}}\rho(\theta,\phi)\,d\theta\,d\phi=1$ and hence, $\rho'(\cdot,\cdot)$ in (20) is also real, positive satisfying

$$\frac{1}{(2\pi)^2}\int_{-2\pi\gamma_y}^{2\pi\gamma_y}\int_{-2\pi\gamma_z}^{2\pi\gamma_z}\rho'(u,v)\,du\,dv=1.$$

So far, we have obtained an upper bound on the first and third terms of (73). Now, we consider the second term on the RHS of (73). To obtain an upper bound on that term, we use the fact that, for a $\mathcal{C}^k$-2-dimensional-periodic function $f(x,y)$, i.e., $f(x,y)$ has k continuous partial derivatives $\frac{\partial^k \vartheta(u,v)}{\partial u^{k_1} \partial v^{k_2}}$ such that $k_1+k_2=k$, the Fourier series coefficients $\{c_{n,m}\}$ decay faster than $\frac{1}{n^{k_1} m^{k_2}}$, that is, $|c_{n,m}| = o(\frac{1}{n^{k_1} m^{k_2}})$, $k_1+k_2=k$. Assuming that $\vartheta'(u,v)$ belongs to $\mathcal{C}^k$, we can write

$$\begin{aligned}
\sum_{(n',m')\in\bar{\mathcal{S}}_{N,M}} |c_{n',m'}| &= \sum_{|n'|\geq N} \sum_{|m'|\geq M} |c_{n',m'}| \\
&+ \sum_{|n'|\geq N} \sum_{|m'|<M} |c_{n',m'}| + \sum_{|n'|<N} \sum_{|m'|\geq M} |c_{n',m'}| \\
&= o(\frac{1}{N^{k_1} M^{k_2}}) + o(\frac{1}{N^k}) + o(\frac{1}{M^k}) \\
&= o\Big(\big(\min(N,M)\big)^{-k}\Big). \qquad (75)
\end{aligned}$$

Using (74) and (75) in (73) yields

$$\begin{aligned}
|\varepsilon_{n,m}^{(dl)}| &\leq 2(2MN - M - N + 1) \\
&\quad \times \Big(1 - \frac{1}{(2\pi)^2} \int_{-\pi}^{\pi} \int_{-\pi}^{\pi} \vartheta(u,v)\, du\, dv\Big) \\
&\quad + o\Big(\big(\min(N,M)\big)^{-k}\Big), \\
&\leq 4MN\Big(1 - \frac{1}{(2\pi)^2} \int_{-\pi}^{\pi} \int_{-\pi}^{\pi} \vartheta(u,v)\, du\, dv\Big) \\
&\quad + o\Big(\big(\min(N,M)\big)^{-k}\Big). \qquad (76)
\end{aligned}$$

■

REFERENCES

[1] S. Elhoushy, M. Ibrahim, and W. Hamouda, "Cell-free massive MIMO: A survey," *IEEE Commun. Surv. Tutorial*, vol. 24, no. 1, pp. 492–523, 2022.

[2] E. Larsson, O. Edfors, F. Tufvesson, and T. Marzetta, "Massive MIMO for next generation wireless systems," *IEEE Commun. Mag.*, vol. 52, no. 2, pp. 186–195, 2014.

[3] X. Yang, F. Cao, M. Matthaiou, and S. Jin, "On the uplink transmission of extra-large scale massive MIMO systems," *IEEE Trans. Veh. Technol.*, vol. 69, no. 12, pp. 15229–15243, 2020.

[4] M. Albreem, M. Juntti, and S. Shahabuddin, "Massive MIMO detection techniques: A survey," *IEEE Commun. Surv. Tutorial*, vol. 21, no. 4, pp. 3109–3132, 2019.

[5] Z. Zhong, L. Fan, and S. Ge, "FDD massive MIMO uplink and downlink channel reciprocity properties: Full or partial reciprocity?," in *Proc. IEEE Glob. Commun. Conf.*, pp. 1–5, 2020.

[6] E. G. Larsson, O. Edfors, F. Tufvesson, and T. L. Marzetta, "Massive MIMO for next generation wireless systems," *IEEE Commun. Mag.*, vol. 52, no. 2, pp. 186–195, 2014.

[7] B. Hassibi and B. M. Hochwald, "How much training is needed in multiple-antenna wireless links?," *IEEE Trans. Inf. Theory*, vol. 49, no. 4, pp. 951–963, 2003.

[8] L. Lu, G. Y. Li, A. L. Swindlehurst, A. Ashikhmin, and R. Zhang, "An overview of massive MIMO: Benefits and challenges," *IEEE J. Select. Topics Signal Processing*, vol. 8, no. 5, pp. 742–758, 2014.

[9] F. S. J. Mirzaei, S. Shahbazpanahi and R. Adve, "Hybrid analog and digital beamforming design for channel estimation in correlated massive MIMO systems," *IEEE Trans. Signal Processing*, vol. 69, pp. 5784–5800, 2021.

[10] A. Sheikhi, S. M. Razavizadeh, and I. Lee, "A comparison of TDD and FDD massive MIMO systems against smart jamming," *IEEE Access*, vol. 8, pp. 72068–72077, 2020.

[11] C. Farsakh and J. Nossek, "Spatial covariance based downlink beamforming in an SDMA mobile radio system," *IEEE Trans. Commun.*, vol. 46, no. 11, pp. 1497–1506, 1998.

[12] J. Goldberg and J. Fonollosa, "Downlink beamforming for spatially distributed sources in cellular mobile communications," *Signal Processing*, vol. 65, no. 2, pp. 181–197, 1998.

[13] M. B. Khalilsarai, S. Haghighatshoar, X. Yi, and G. Caire, "FDD massive MIMO via UL/DL channel covariance extrapolation and active channel sparsification," *IEEE Trans. Wireless Commun.*, vol. 18, pp. 121–135, Nov. 2019.

[14] M. B. Khalilsarai, Y. Song, T. Yang, S. Haghighatshoar, and G. Caire, "Uplink-downlink channel covariance transformations and precoding design for FDD massive MIMO," in *Asilomar*, (Pacific Grove, CA, USA, USA), pp. 199–206, Nov. 2019.

[15] H. Xie, F. Gao, S. Jin, J. Fang, and Y. Lian, "Channel estimation for TDD/FDD massive MIMO systems with channel covariance computing," *IEEE Trans. Wireless Commun.*, vol. 17, pp. 4206–4218, Apr. 2018.

[16] L. Miretti, R. L. G. Cavalcante, and S. Stanczak, "Channel covariance conversion and modelling using infinite dimensional Hilbert spaces," *IEEE Trans. Signal Processing*, pp. 3145–3159, 2021.

[17] M. Jordan, A. Dimofte, X. Gong, and G. Ascheid, "Conversion from uplink to downlink spatio-temporal correlation with cubic splines," in *VTC Spring 2009 - IEEE 69th Vehicular Technology Conference*, (Barcelona, Spain), pp. 1–5, Apr. 2009.

[18] Y.-C. Liang and F. P. S. Chin, "Downlink channel covariance matrix (DCCM) estimation and its applications in wireless DS-CDMA systems," *IEEE J. Select. Areas Commun.*, vol. 19, pp. 222–232, Feb. 2001.

[19] A. Decurninge, M. Guillaud, and D. T. M. Slock, "Channel covariance estimation in massive MIMO frequency division duplex systems," in *Proc. IEEE Glob. Commun. Conf.*, (San Diego, CA, USA), pp. 1–6, Dec. 2015.

[20] L. Miretti, R. L. Cavalcante, and S. Stanczak, "Downlink channel spatial covariance estimation in realistic FDD massive MIMO systems," *2018 IEEE Global Conf. Signal Inf. Processing (GlobalSIP)*, Nov. 2018.

[21] P. E. M. K. I. Pedersen and B. H. Fleury, "A stochastic model of the temporal and azimuthal dispersion seen at the base station in outdoor propagation environments," *IEEE Trans. Veh. Technol.*, vol. 49, no. 2, pp. 437–447, 2000.

[22] P. Butzer, *A Survey of the Whittaker-Shannon Sampling Theorem and Some of Its Extensions*. Lehrstuhl A für Math., Rheinisch-Westfälische Techn. Hochsch., 1982.

[23] S. Haghighatshoar, M. B. Khalilsarai, and G. Caire, "Multi-band covariance interpolation with applications in massive MIMO," in *Proc. IEEE Int. Symp. Inf. Theory*, pp. 386–390, 2018.

[24] A. Adhikary, J. Nam, J. Ahn, and G. Caire, "Joint spatial division and multiplexing-the large-scale array regime," *IEEE Trans. Inf. Theory*, vol. 59, no. 10, pp. 6441–6463, 2013.

[25] A. F. Molisch, *Wireless Communications*. Wiley Publishing, 2nd ed., 2011.

[26] L. You, X. Gao, X. G. Xia, N. Ma, and Y. Peng, "Pilot reuse for massive MIMO transmission over spatially correlated rayleigh fading channels," *IEEE Trans. Wireless Commun.*, vol. 14, no. 6, pp. 3352–3366, 2015.

[27] Z. Yun and M. F. Iskander, "Ray tracing for radio propagation modeling: Principles and applications," *IEEE Access*, vol. 3, pp. 1089–1100, 2015.

[28] M. Koller, C. Hellings, and W. Utschick, "Learning-based channel estimation for various antenna array configurations," in *2019 IEEE 20th Int. Wksp. Signal Processing Adv. Wireless Commun. (SPAWC)*, pp. 1–5, 2019.

[29] A. Poularikas, *Handbook of Formulas and Tables for Signal Processing*. CRC Press, 1998.